Int. J. Electrochem. Sci., 16 **(2021)** Article Number: 211151, doi: 10.20964/2021.11.53

International Journal of
ELECTROCHEMICAL
SCIENCE
www.electrochemsci.org

Investigation of Failure Behavior of HRB335 steel due to Crevice Corrosion in Concrete Using Electrochemical Method

Gang Li, Di Yin, Jianrong Pang

College of Civil Engineering, Cangzhou Jiaotong College, Hebei Cangzhou 061199, China
*E-mail: teacher_li08@163.com

Received: 21 August 2021 / *Accepted:* 17 September 2021 / *Published:* 10 October 2021

The corrosion of reinforcements in the concrete crevice is a crucial factor affecting the safety and stability of concrete, especially in an environment containing chloride ions. Cathodic protection is one of the key methods to protect reinforcements in concrete. In this paper, based on wedge crevice corrosion experimental device, the corrosion behaviour of reinforcement in concrete crevice structure and the effectiveness of cathodic protection were studied involving electrochemical parameters, corrosion rate and electrochemical impedance spectroscopy. The results showed that the anode area was located near the opening. With the development of the crevice depth, the corrosion form changed from general corrosion to pitting corrosion and from the anode area to the cathode area. The cathodic protection made the anode area move forward in the crevice, intensified the corrosion degree of the anode area, and pitted corrosion at sample 6# in the deepest crevice.

Keywords: Concrete; Cathodic protection; Electrochemical method; Wedge crevice device

1. INTRODUCTION

Reinforced concrete is the primary engineering material of civil engineering structures. With the massive construction of highways, bridges and other infrastructures, more and more concrete structures are constructed in extreme environments, including the marine or alpine environment, which puts forward higher requirements regarding the durability of reinforced concrete structures [1-3].

At present, whole-hole prefabricated box-girder bridge erection technology is mainly used in bridge construction. However, the concrete at the connection part of precast members of prefabricated bridges has a layer of cement mortar matrix, which is far less dense than the concrete body, forming a particular problem of steel bar corrosion in the cracks of the prefabricated and post-poured concrete interface [4]. The key to the durability of precast and post-cast concrete interface zone could be the

effect of chloride ion transport and the corrosion characteristics of steel bars across the boundary [5]. These could have important practical significance for protecting the existing whole-hole precast box girder bridge structure and the design of future bridge structures.

The erosion of concrete by chloride ions mainly occurs in the marine environment. Chloride ions gather on the concrete surface with the solution and diffuse into the interface area of prefabricated and post-cast concrete through a particular physical activity [6,7]. Then it accumulates on the steel surface, causing steel corrosion and leading to durability failure of the steel-concrete structure.

For reinforced concrete structures exposed to the atmosphere, cathodic protection is ideal for preventing steel corrosion, especially suitable for local pitting of steel bars due to chloride [8]. It can reduce the corrosion of steel bars by raising the pH of the steel/concrete interface, reducing the Cl^- concentration near the damaged passivation film. However, further research is needed due to the shielding effect of the gap structure on cathodic protection and the problem of the protection distance of cathodic protection in the gap under the conditions of different environmental temperatures.

In this paper, based on wedge crevice corrosion experimental device, the corrosion behaviour of reinforcement in concrete crevice structure and the effectiveness of cathodic protection were studied, involving electrochemical parameters, corrosion rate and electrochemical impedance spectroscopy.

2. EXPERIMENTAL SETTINGS

A wedge crevice experimental device was used to simulate the crack structure in concrete (Fig.1). The cover plates were made of transparent PE (Poly Ethylen) material, and the gap angle was 1° (with a gap width of ≈0.3 mm). A test sample was arranged at the opening, and 5 test samples were arranged at 3-15 cm away from the opening, named as 0 - 1#，3 cm - 2#，6 cm - 3#，9 cm - 4#，12 cm - 5# and 15 cm - 6#, respectively. According to the protocol during the electrochemical tests, a reference electrode and an auxiliary electrode were set at each test piece location to investigate the variation of corrosion dynamics parameters of the samples, including corrosion potential (E_{corr}) and galvanic current density (I_{corr}), where the sample with "+" I_{corr} was the anode and the one with "-" I_{corr} was the cathode. The applied DC (Direct Current) source realized the cathodic protection of the experimental device, and the auxiliary anode was the Pt electrode. Different cathodic polarization potentials (CP) were achieved by adjusting the variable resistance and DC power output. The potential of the test sheet calibrated the as-applied CP at the beginning of the measurements.

The sample material was HRB335 steel, and the size was 10×10×2 mm^3. The main components are detailed in Tab.1. Before the experiment, each sample was cleaned with acetone, alcohol and deionized water successively [9]. After drying, a wire was welded on the back of the sample for testing the electrochemical parameters. Before the experiment, the sample's test surface was polished to the mirror surface to reduce the experimental error caused by the rough surface of the samples.

(1) Study on crevice corrosion and CP shield

The effect of the seawater environment on the corrosion of steel bars in concrete holes was simulated using the experimental solution with wt.3.5% NaCl solution prepared by pure NaCl and deionized water. Considering the influence of temperature on the corrosion behaviour of HRB335 steel

in the concrete crevice [9], the experimental temperatures were set at 20℃, 50℃ and 80℃, respectively.

Taking the potential of the sample as the reference, the CP of -100 mV, -200 mV and -300 mV were set by the DC source, and the change of sample potential at other positions was monitored to analyze the shielding effect of the concrete crevice structure on CP. For the immersion experiment, the contrast experiment was set as two conditions of No CP and CP = -300 mV, and the immersion experiment was carried out for 24 h. The samples' general corrosion rate and macro corrosion morphology at different positions were analyzed, and the effectiveness of CP in concrete crevice structure was analyzed.

The whole set of the experimental device was placed in a constant temperature - humidity apparatus. After the whole experimental device was stabilized for 2 h, it was continuously tested for 10 min to obtain 600 experimental data points, and the average value was taken for analysis.

(2) Study on evolution of corrosion process inside crevice under cathodic protection

Taking the 6# sample as an example, the 24-hour immersion experiment was carried out to reveal the mechanism of cathodic protection on crevice corrosion by comparing the change law of electrochemical impedance characteristics with/without cathodic protection.

Table 1. Main components of HRB335 steel (wt.%)

Element	C	Si	Mn	P	S	Ceq
Content	0.25	0.80	1.60	0.045	0.045	0.52

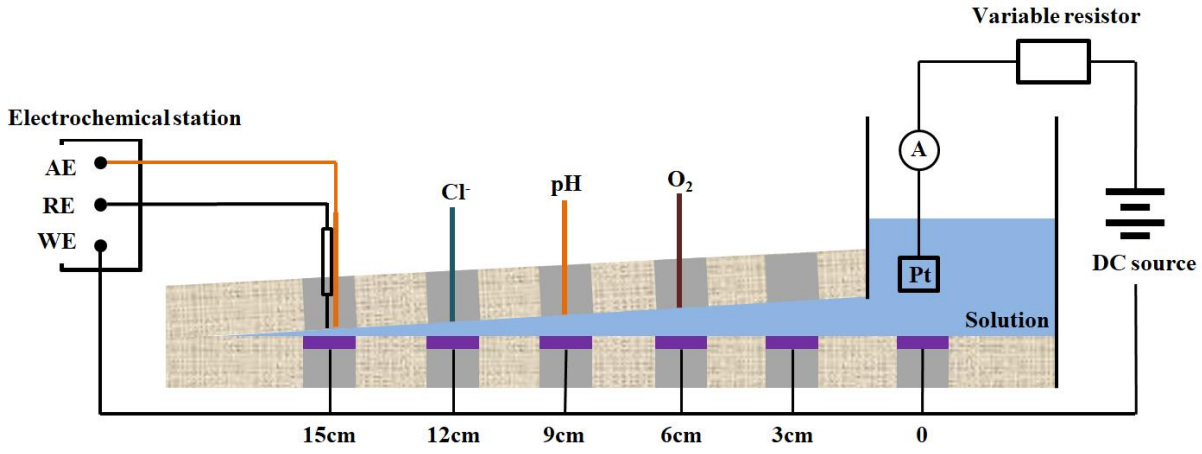

Figure 1. Wedge crevice experimental device for simulating concrete crevice with six test samples (1#-6#) immersing in wt.3.5% NaCl solution at 20℃, 50℃ and 80℃

3. RESULTS AND DISCUSSION

3.1 Potential and galvanic current distribution in the concrete crevice

Fig.2 shows the samples' potential and galvanic current distribution at different positions of 3-15 cm away from the opening under different temperatures (20℃, 50℃ and 80℃). At the beginning of the corrosion experiment, the oxygen was sufficient along the crevice, at which the oxygen depolarization process controlled the corrosion process at a different location [10-12]. With the progress of the experiment, the oxygen inside the crevice was exhausted. Due to the closed structure of the crevice, it was difficult for the oxygen to diffuse to the inside crevice. Thus, the oxygen concentration difference battery with the crevice inside as anode and the crevice outside as cathode was formed [13]. According to the electrochemical test investigations, the change rules of corrosion potential and galvanic current density of the samples did not change at different temperatures, indicating that the temperature did not significantly affect the crevice corrosion mechanism [14]. However, differently from the previously drawn conclusions, compared with the 1# sample, the E_{corr} of the 2# sample had a significant negative deviation. Moreover, the E_{corr} of the samples showed a positive deviation with the increase of the crevice depth. As can be seen from the I_{corr} results, the higher temperature caused higher I_{corr} values, indicating the more severe corrosion. However, the anodes in the crevice appeared at the positions of samples 3#, 4# and 5#, and the samples 1#, 2# and 6# worked as cathodes. In the oxygen concentration difference theory in crevice corrosion, the deeper the crevice induced an accentuated corrosion. It was also found that the most severe corrosion occurs at 3# based on the value of I_{corr}. Furthermore, with the increase of the crevice depth for the 3# sample, the corrosion weakened, and the 6# sample behaved as the cathode [15-17]. Therefore, to explore the causes of this phenomenon, the macro morphology of metal corrosion at different locations was analyzed at 80℃ as an example (Fig.3).

As mentioned above, 1# and 2# samples near the opening were in the cathode region. Figure 3 shows that the metal surfaces of 1# and 2# samples were non-corroded, and the surfaces were smooth and uniform. With the increase of the crevice depth, the samples 3# and 4# showed a general corrosion form, but the corrosion degree of the 3# was much greater than that of the 4#, proved by the $I_{corr\text{-}3\#} > I_{corr\text{-}4\#}$. When the crevice depth reached sample 5#, the corrosion morphology gradually showed an aggregation trend [18]. Moreover, it changed the local corrosion characteristics with the minimum anode current density, and thus an apparent pitting morphology was observed at sample 6#. Therefore, the same as the original crevice corrosion theory, the crevice corrosion showed the oxygen concentration difference theory [19,20]. However, the most severe corrosion position was not found in sample 6# in the deepest crevice. At the same time, with the increment of the crevice depth, the corrosion form changed from general corrosion to pitting corrosion and from the anode to the cathode.

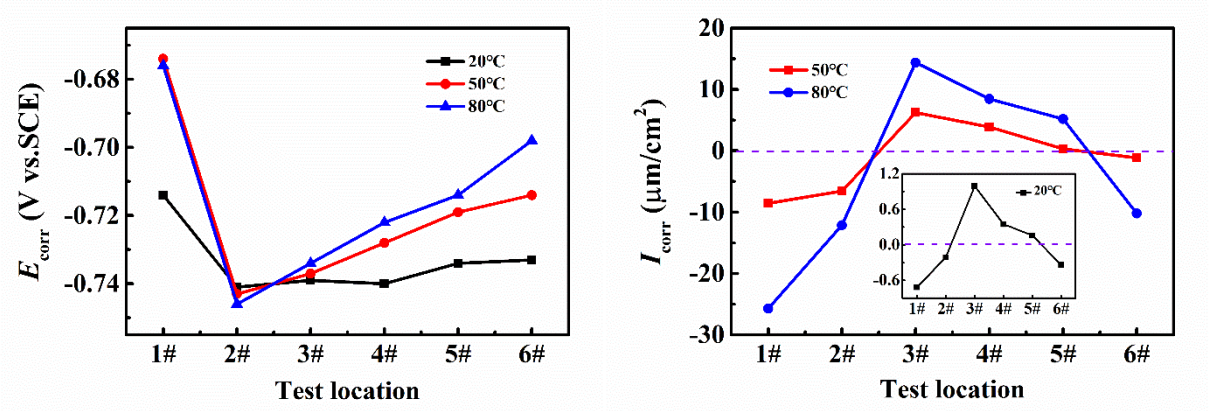

Figure 2. The corrosion potential (E_{corr}) and galvanic current density (I_{corr}) of HRB335 steel at different locations of 0-15 cm (1#-6# sample) away from the opening after immersing in wt.3.5% NaCl solution for 2 h at 20℃, 50℃ and 80℃ using wedge crevice experimental device

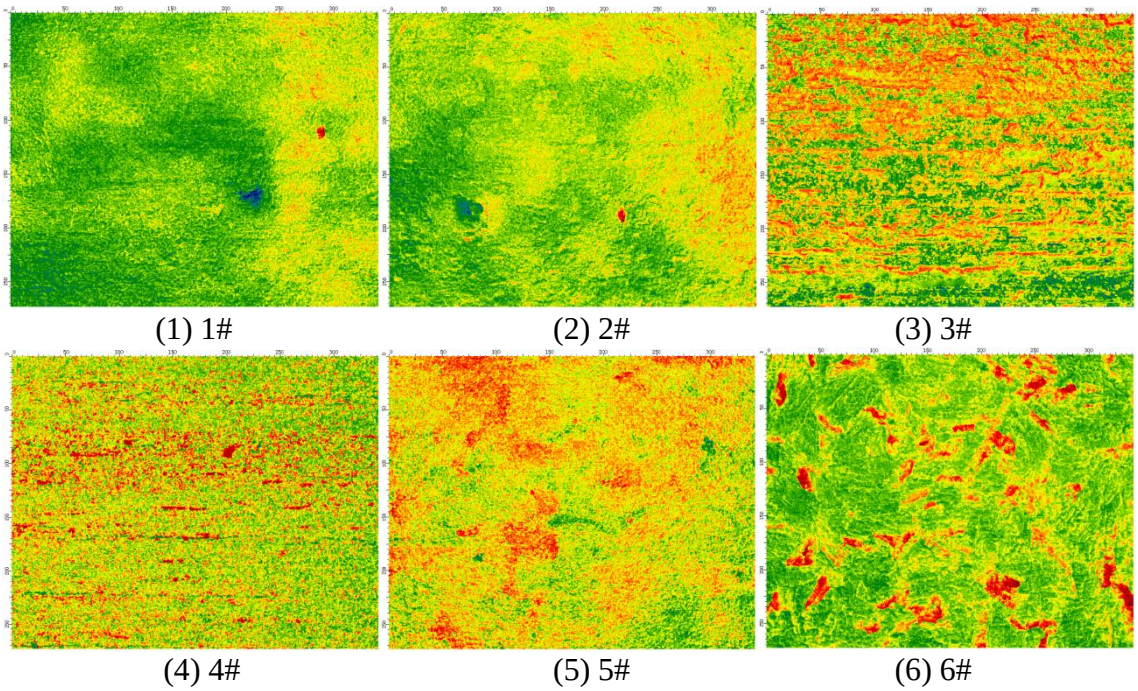

Figure 3. Macro corrosion morphology of HRB335 steel at different locations of 0-15 cm (1#-6# sample) away from the opening after immersing in wt.3.5% NaCl solution for 2 h at 80℃ using wedge crevice experimental device

3.2 CP shielding of the concrete crevice

Different polarisation potentials were applied under different temperature conditions to study the shielding effect of concrete crevice structure on cathodic protection. After a stabilization lasting for 2 h, the polarization potentials of samples at different positions were tested (Fig.4). The polarization potential of samples decreased with the increase of crevice depth, indicating the shielding effect of crevice structure on cathodic protection. Simultaneously, the higher the temperatures induced smaller the potential drops along with the crevice depth [21]. The potential curve at 50℃ and 80℃ was in

coincidence, indicating that the temperature can effectively promote the diffusion process of ions into the crevice, promoting the protection range of the cathodcic current [22]. However, no further change will occur when the temperature increases to a certain degree (50℃).

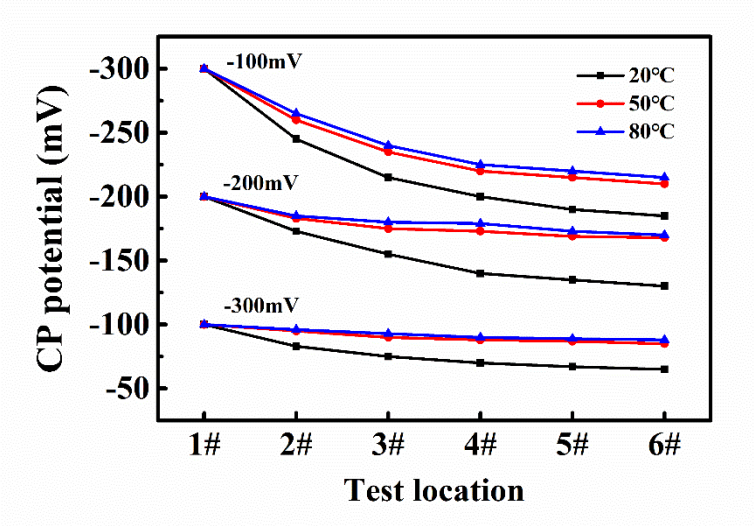

Figure 4. Cathodic polarization potential of polarized HRB335 steel with CP = -100 mV, -200 mV and 300 mV at different locations of 0-15 cm (1#-6# sample) away from the opening after immersing in wt.3.5% NaCl solution for 2 h at 20℃, 50℃ and 80℃ using wedge crevice experimental device

The influence of applied cathodic potential on the corrosion rate of samples in different positions was investigated. Fig.5 showed general corrosion rates of samples at different positions with/without cathodic protection of -300 mV. It can be seen that the general corrosion rate of samples 2#, 3# and 4# increased applying a CP = -300 mV, while the general corrosion rate of 1#, 5# and 6# samples decreased. By comparing the Icorr distribution results in Fig.2 without cathodic protection, the 3#, 4# and 5# samples were the anodes, while the 1#, 2# and 6# samples were the cathodes. However, the anode area moved forward to 2#, 3# and 4# samples with CP = -300 mV. Fig.6 shows the comparison of macro corrosion morphology of the samples with/without CP = -300 mV. During the experiment, the serious corrosion positions were concentrated in samples 3#, 4# and 5# without CP = -300 mV, consistent with the analysis results of Fig.2. However, the corrosion of 2# sample occurred at 2.5 h with CP = -300 mV, and the corrosion morphology of 2# and 3# samples was significantly more severe than that without cathodic protection [23]. The corrosion morphology of 5# and 6# samples was slightly compared with that without cathodic protection. The change rule of the general corrosion rate was consistent with Fig.5.

The corrosion mechanism for crevice corrosion with cathodic protection was similar to that of non-cathodic protection concrete crevice, where differences in the oxygen concentration controlled the corrosion. The corrosion products accumulated in the anodic area promoted the formation of the block area [24]. The excess Fe^{2+} promoted the eternal Cl^- inward migration, and then hydrolysis of Fe^{2+}

resulted in acidification of the block area, which accelerated the dissolution of the anode. Furthermore, when cathodic protection was applied, cathodic polarization in the initial stage provided free electrons [25]. At the same time, dissolved oxygen was consumed faster in the concrete crevice to accelerate the anodization process and promote the general corrosion area forward. This strengthened the block degree in the concrete crevice and aggravated the pitting corrosion inside the crevice, indicating more severe corrosion than without cathodic protection [26].

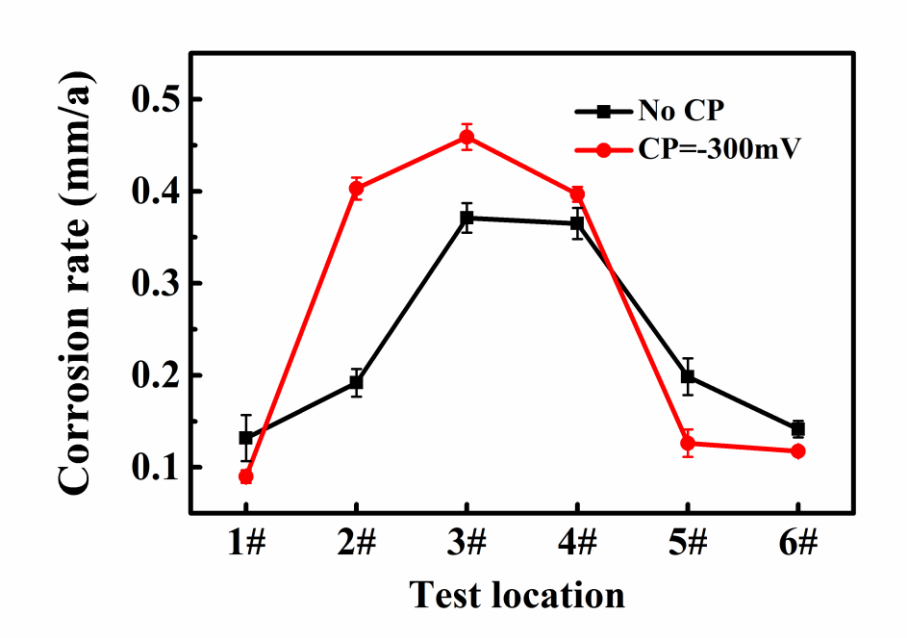

Figure 5. General corrosion rates of HRB335 steel with / without CP = -300 mV at different locations of 0-15 cm (1#-6# sample) away from the opening after immersing in wt.3.5% NaCl solution for 24 h at 80℃ using wedge crevice experimental device

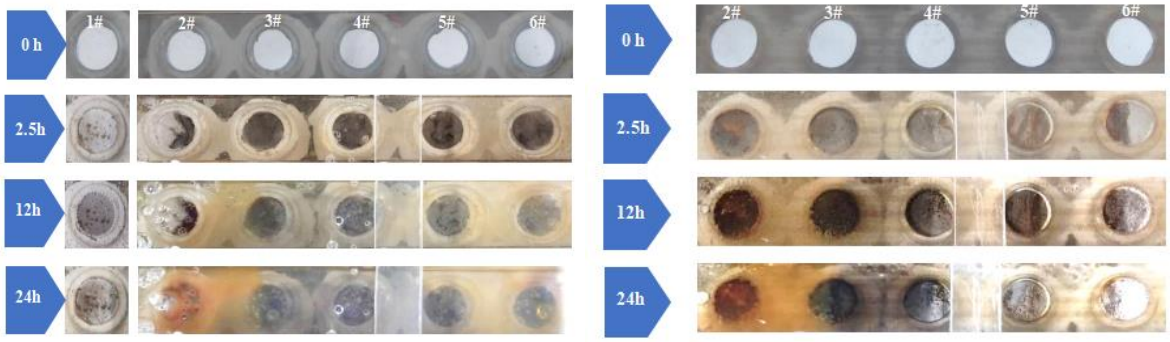

(1) No CP (2) CP = -300 mV

Figure 6. Corrosion morphology of HRB335 steel with / without CP = -300 mV at different locations of 0-15 cm (1#-6# sample) away from the opening after immersing in wt.3.5% NaCl solution for 24 h at 80℃ using wedge crevice experimental device

3.3 Development of corrosion inside crevice

Sample 6# was chosen as an example to carry out investigations dealing with electrochemical impedance spectroscopy (EIS) to analyze the influence of cathodic protection on the corrosion behaviour inside the crevice. The EIS curves of sample 6# sample with/without CP = -300 mV are presented in Fig.7. The corrosion of all samples at different locations behaved as activated corrosion, so the equivalent circuit was chosen as $R_s(Q(R_p(C_{dl}R_{ct}))$: where R_s was solution resistance, Q was the capacitor, R_p was the polarization resistance of corrosion product film, C_{dl} was double electric layer capacitor, and R_{ct} was the charge transfer resistance.

As shown from Fig.7, in the initial experimental time at 1 h, the impedance arc characteristics in Nyquist diagrams were relatively complete, and the arc radius with CP = -300 mV was larger than that without cathodic protection. Cathodic protection made the surface resistance larger and the corrosion rate smaller [27]. The Nyquist impedance radius decreased significantly with experimental time, indicating that the corrosion rate was accelerated, especially at the transition stage from 1 h to 3 h. The corresponding Bode plots showed the same variation characteristics. In log*f*-|*Z*| curves, the high frequency (10^5 Hz) and low resistance (10^{-2} Hz) all decreased with the increase of experimental time [28]. In contrast, the mass diffusion impedance of 6# sample first decreased rapidly after slowed down and smaller than that without cathodic protection at 24 h. The structure of corrosion products on the surface of sample 6# with CP = -300 mV was loose. On the one hand, the corrosion products were more likely to diffuse. On the other hand, the porous corrosion product layer was more likely to absorb Cl^- and promote the local corrosion, intensifying the pitting corrosion of the sample.

Tab.2 collects the results of EIS curves of sample 6#. It can be seen that the capacitance (Q) and polarization resistance of corrosion product film (R_p) representing the surface characteristics showed significantly different values due to the application of cathodic protection [29]. However, the cathodic protection did not influence the changing trends of electric double-layer capacitance (C_{dl}) and charge transfer resistance (R_{ct}), representing the electrochemical corrosion process. It was indicated that the corrosion process of the 6# sample was unchanged, and the structure of the corrosion product film was different.

The corrosion product on the surface of sample 6# was mainly $Fe(OH)_2$ without cathodic protection. During the long soaking process, the $Fe(OH)_2$ layer dissolved and broke, which led to the matrix of the 6# sample gradually appearing again [30]. The capacitance (Q) increased slowly firstly and then rapidly. The polarization resistance (R_p) increased rapidly due to the accumulation of $Fe(OH)_2$ on the sample surface in the early experimental process and decreased due to the diffusion of dissolution and rupture. At the same time, in the early experimental stage, the corrosion process was mainly pitting corrosion because of the $Fe(OH)_2$ coverage. Thus, the double electric layer capacitance (C_{dl}) was small and remained unchanged during a long experimental time. As the sample matrix was exposed to the solution again and accelerated the corrosion, the C_{dl} enlarged rapidly. Therefore, the charge transfer resistance (R_{ct}) rapidly decreasing first and then slowly decreased.

When the cathodic polarization was applied, the potential difference between anode and cathode increased. Moreover, the corrosion rate of sample 6# and the hydrolysis rate of Fe^{2+} were accelerated, and a large amount of Cl^- moved inwardly, forming the porous structure of γ-FeOOH.

Therefore, the capacitance (Q) was high and changed little during the long experimental process because the porous structure can promote the diffusion of corrosive media. A large amount of $[Fe(H_2O)]Cl_3$ was also generated continuously, filling the porous structure. Thus, the polarization resistance (R_p) dropped continuously and increased slightly when the porous structure was filled to a particular state. However, the sample matrix was always directly exposed to the corrosive medium, so the double electric layer capacitor C_{dl} and charge transfer resistance R_{ct} had the same variation law with the related parameters of the sample 6# without cathodic protection.

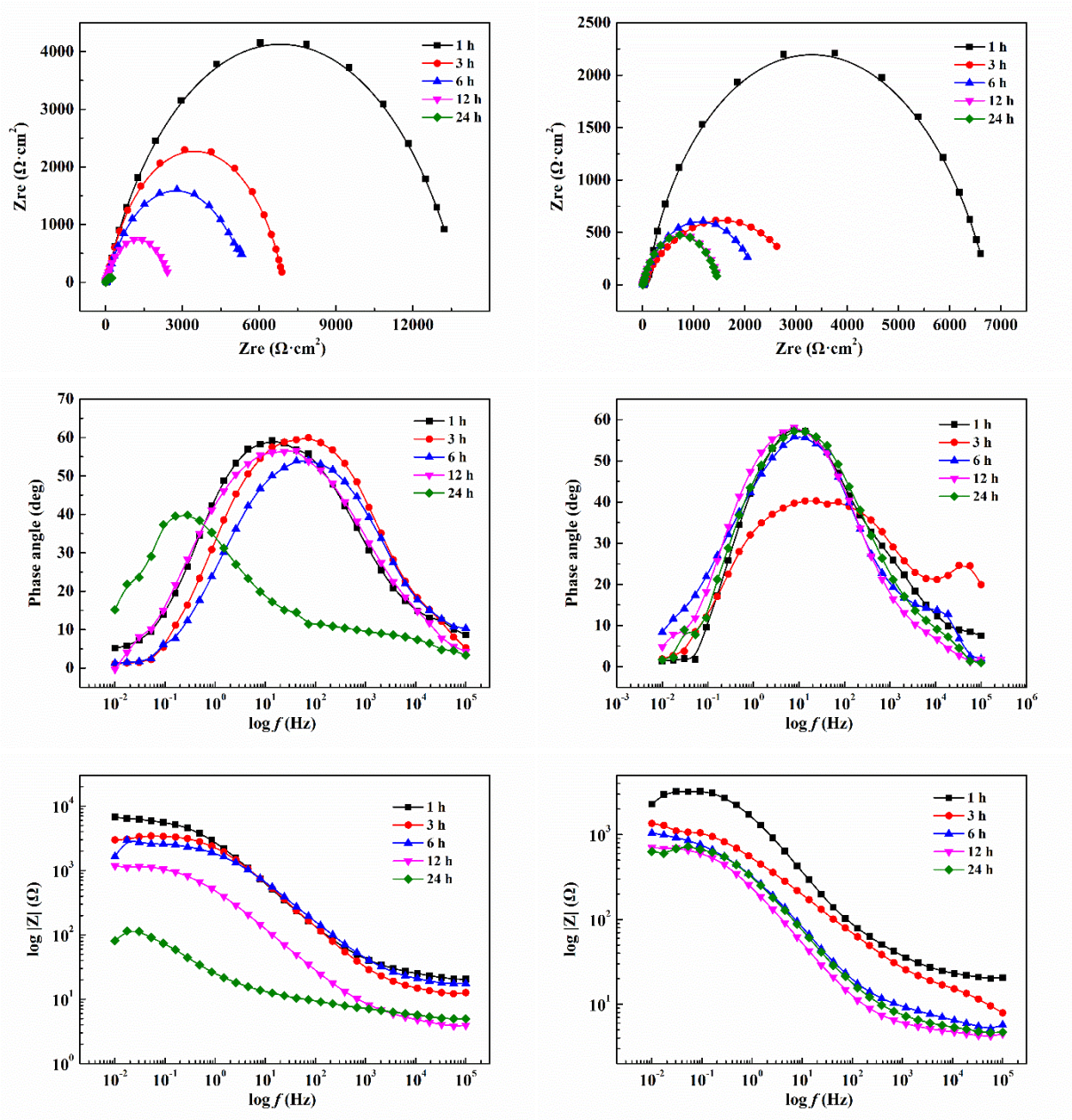

(1) CP = -300 mV (2) No CP

Figure 7. The EIS curves of 6# sample over experimental time with / without CP = -300 mV after immersing in wt.3.5% NaCl solution for 24 h at 80℃ using wedge crevice experimental device

Table 2. The fitting results of EIS curves of 6# sample with / without CP = -300 mV after immersing in wt.3.5% NaCl solution for 24 h at 80℃ using wedge crevice experimental device

Time \ Parameter		R_s ($\Omega \cdot cm^2$)	Q (F/cm^2)	n	R_p ($\Omega \cdot cm^2$)	C_{dl} (F/cm^2)	R_{ct} ($\Omega \cdot cm^2$)
CP = -300 mV	1 h	40.20	3.87×10^{-5}	0.68	3.06×10^{1}	1.77×10^{-6}	1.35×10^{4}
	3 h	24.30	3.91×10^{-5}	0.74	2.45×10^{3}	1.99×10^{-6}	4.49×10^{3}
	6 h	33.00	3.92×10^{-5}	0.68	3.83×10^{3}	1.85×10^{-3}	2.54×10^{3}
	12 h	7.80	2.20×10^{-4}	0.67	1.59×10^{1}	4.82×10^{-6}	2.36×10^{3}
	24 h	9.70	5.70×10^{-4}	0.41	3.77×10^{1}	2.48×10^{-2}	3.80×10^{2}
No CP	1 h	40.50	4.94×10^{-5}	0.69	3.00×10^{2}	8.09×10^{-6}	6.42×10^{3}
	3 h	12.20	2.86×10^{-4}	0.47	2.81×10^{2}	4.05×10^{-5}	2.93×10^{3}
	6 h	10.60	3.97×10^{-4}	0.60	2.62×10^{2}	2.37×10^{-5}	2.25×10^{3}
	12 h	8.91	4.54×10^{-4}	0.70	5.45×10^{0}	2.11×10^{-5}	1.46×10^{3}
	24 h	9.73	3.00×10^{-4}	0.70	8.32×10^{1}	2.06×10^{-4}	1.41×10^{3}

4. CONCLUSION

Based on the wedge crevice corrosion experimental device, the corrosion behaviour of reinforcement in concrete crevice structure and the influence of cathodic protection on crevice corrosion was studied through electrochemical parameters, corrosion rate and electrochemical impedance testing. The main conclusions were as follows:

(1) The crevice corrosion showed the oxygen concentration difference theory. However, the anode area was located near the opening, while the sample 6# in the deepest crevice behaved as a cathodic region. Simultaneously, with the development of the crevice depth, the corrosion form changed from general corrosion to pitting corrosion and from the anodic to the cathodic area.

(2) Crevice structure had a certain shielding effect on cathodic protection, and the smaller the temperature was, the greater the shielding effect was. The cathodic protection made the anode area move forward in the crevice, intensified the corrosion degree of the anode area and the pitting corrosion at 6# sample in the deepest crevice.

Referneces

1. R.D. Moser, P.M. Singh, L.F. Kahn, K.E. Kurtis, D.G. Nino and Z.B. Mcclelland, *Constr. Build. Mater.*, 203 (2019) 366.
2. C. Yang, Q. Han, A.Q. Wang, Y. Yang and X.Y. Li, *AIP Adv.*, 11 (2021) 035217.
3. E. Redaelli and L. Bertolini, *Mater. Corros.*, 66 (2015) 756.
4. A. Goyal, H.S. Pouya, E. Ganjian, A.O. Olubanwo and M. Khorami, *Constr. Build. Mater.*, 194 (2019) 344.
5. C. Yang, G.J. Wang, Q. Han, H.B. Liu, A.Q. Wang and L. Sun, *Int. J. Electrochem. Sci.*, 16 (2021) 210365.
6. H. Al-Mattarneh, *Corros. Sci.*, 105 (2016) 133.
7. W. Vélez, F. Matta, P. Ziehl, *Mater. Struct.*, 49 (2016) 507.
8. Y.Z. Mao, Y.H. Wei, H.T. Zhao, C.X. Lv, H.J. Cao and J. Li, *Acta Metall. Sin-Engl.*, 31(2018) 1171.

9. B. Dubose, *Mater. Performance*, 56 (2017) 17.
10. F.M. Al Mutlaq and C.L. Page, *Constr. Build. Mater.*, 39 (2013) 60.
11. J. Shen, G.L. Song, D.J. Zheng and Z.M. Wang, *Mater. Corros.*, 70 (2019) 2228.
12. J.Wei, X.X. Fu, J.H. Dong and W. Ke, *J. Mater. Sci. Technol.*, 10 (2012) 43.
13. U. Angst U, *Electrochim. Acta*, 56 (2011) 5877.
14. B. Elsener, D. Addari, S. Coray and A. Rossi, *Mater. Corros.*, 62 (2011) 111.
15. S. Soleimani, P. Ghods, O.B. Isgor and J. Zhang, *Cement Concrete Comp.*, 32 (2010) 360.
16. W. Wang, K. Shen, J. Yi and Q. Wang, *J. Loss. Prevent Proc.*, 41 (2016) 270.
17. C. Xu, F. Gao, Y. Wang and C. He, *Mater. Design*, 89 (2016) 196.
18. M. Grabowski and S. Virtanen, *Corrosion*, 73 (2017) 563.
19. S. Qian and Y.F. Cheng, *Constr. Build. Mater.*, 148 (2017) 675.
20. F. Varela, M.Y.J. Tan and M. Forsyth, *Electrochim. Acta*, 186 (2015) 377.
21. I. Gurrappa, I.V.S. Yashwanth and I. Mounika, *P. Natl. A. Sci. India A.*, 85 (2015) 1.
22. Q. Li, D. Zeng and M. An, *Chem. Phys. Lett.*, 722 (2019) 1.
23. F.M. Song, *Corros. Sci.*, 55 (2012) 107.
24. F.M. Song, *Electrochim. Acta*, 56 (2011) 6789.
25. R. Montoya, F.R. Garcia-Galvan, A. Jimenez-Morales and J.C. Galvan, *Corros. Sci.*, 82 (2014) 432.
26. L.Y. Xu and Y.F. Cheng, *Corros. Sci.*, 78 (2014) 162.
27. G.S. Steeb and R. Tank, *Mater. Corros.*, 60 (2015) 344.
28. N. Kr. Prasad, A.S. Pathak, S. Kundu, P. Panchal and K. Mondala, *J. Mater. Res. Technol.*, 14 (2021) 582.
29. H.M. Oleiwi, W. Yu, M. Curioni, X. Chen and I.L. Shabalin, *Mater. Struct.*, 51 (2018) 148.
30. P. Lambert, C.V. Nguyen, P.S. Mangat, F.J. O'Flaherty and G. Jones, *Mater. Struct.*, 48 (2015) 2157.